Supercooling of water confined in reverse micelles

2008 J. Phys.: Condens. Matter 20 104204

(http://iopscience.iop.org/0953-8984/20/10/104204)

IOP PUBLISHING JOURNAL OF PHYSICS: CONDENSED MATTER

J. Phys.: Condens. Matter **20** (2008) 104204 (6pp) doi:10.1088/0953-8984/20/10/104204

Supercooling of water confined in reverse micelles

T Spehr[1,2], B Frick[1], I Grillo[1] and B Stühn[2]

[1] Institut Laue Langevin, BP 156, 38042 Grenoble Cedex 9, France
[2] TU Darmstadt, 64289 Darmstadt, Germany

E-mail: spehr@ill.fr

Received 13 July 2007, in final form 29 August 2007
Published 19 February 2008
Online at stacks.iop.org/JPhysCM/20/104204

Abstract

We report on the temperature dependence of the nanosecond-timescale dynamics of the ternary mixture water/AOT/oil with deuterated heptane, toluene or decane as the oil. Water-swollen reverse micelles as formed in such microemulsions allow us to investigate the freezing behaviour of water confined in a soft environment. We report here on the first neutron scattering studies in which the freezing of the confined water and of the oil is followed down to temperatures at which the whole system is frozen. We focus on studies of water confined in three different droplet sizes: by means of small-angle neutron scattering we have determined the radii to be 46, 18, and 7 Å for water to surfactant ratios $\omega = 40$, 12, and 3. From elastic temperature scans by neutron backscattering we deduce a strong supercooling of water confined in the reverse swollen micelles which increases with decreasing droplet size. For the smallest droplets we find a supercooling of more than 45 K compared to bulk water.

1. Introduction

The influence of spatial confinement on the dynamics of liquids is of interest for both fundamental understanding and applications (Koza *et al* 2007). One question is if the existence of a minimal spatially limited region is needed within which cooperative molecular arrangements allow a local motion to take place. For glass-forming liquids this might explain the divergence of the viscosity upon cooling, because such regions are supposed to grow with decreasing temperature, which in consequence should lead to a drastic slowing down of the relaxation times until the glass transition occurs. Such a scenario might be verified by enclosing a liquid in a pore and thereby limiting the spatial extension of a hypothetical cooperative region (Morineau *et al* 1999). The effects of confinement on freezing and melting have attracted special interest (Christenson 2001, Alba-Simionesco *et al* 2006). However, in recent years the great importance of wall interactions became evident, and with this the interest to modify the wall properties either by coating the mesoporous host walls or more recently by studying liquids enclosed within soft walls, e.g. in microemulsion droplets (Wang *et al* 2004). Even though it is not clear whether water undergoes a glasslike freezing or crystallizes in the small droplets investigated here, the case of water as an enclosed liquid in reverse micelles is of special interest because of its importance for biological systems. Microemulsions are thermodynamically stable homogeneous mixtures of a polar and an apolar liquid and amphiphilic molecules called surfactants. In the present study we examined the ternary mixture of water, bis(2-ethyl-hexyl) sulfosuccinate (AOT), and oil, which is known to form a droplet phase over a wide range of compositions (Kotlarchyk *et al* 1984). Small spherical water droplets surrounded by a monolayer of AOT are dispersed in the oil matrix. As the size of the droplets depends to a first approximation only on the molar ratio ω of water to surfactant molecules (Kotlarchyk *et al* 1984), one can continuously change the droplet diameter. Droplets with water core radii ranging from a few angstroms to several nanometres can be obtained. Such small droplet sizes make microemulsions suitable for the investigation of water in soft confinement, and possibly can mimic biological conditions.

In this paper we present the first step of the study of reverse micelle confined water. After describing the experimental conditions and methods we report on the characterization of the investigated systems by small-angle neutron scattering (SANS), which is an excellent tool for studies on structure and interaction in micellar systems (Chen 1986). We then investigate the freezing behaviour of water by probing the energy-resolved elastic scattering on the nanosecond timescale by neutron backscattering (BS) spectrometers.

2. Experimental details

2.1. Samples and materials

The microemulsions were prepared by mixing appropriate amounts of bis(2-ethyl-hexyl) sulfosuccinate (AOT), water, and deuterated oil (decane, heptane or toluene) and shaking for several minutes until the samples were single phase and optically clear. Deuterated solvents n-decane-d22, n-heptane-d16, and toluene-d8 (Euriso-Top, 98%) and AOT (Acros Organics) were used without further purification. Water was of ultrahigh purity (Millipore Milli-Q Plus system). The composition of the microemulsion is given by the two parameters ω and ϕ, with ω being the molar ratio of water to surfactant AOT and ϕ the droplet (water plus AOT) volume fraction. In this study ϕ was kept constant at 0.2 while varying ω between 3 and 40. For a variation of scattering contrast samples with deuterated AOT[3], water and n-decane-d22 were prepared with $\omega = 40$ and 12.

2.2. Small-angle neutron scattering

Small-angle neutron scattering (SANS) experiments were carried out on the instrument D11 at the Institute Laue Langevin (ILL, Grenoble, France) using a neutron wavelength of $\lambda = 4.6$ Å. Three configurations were used to cover a range of scattering vectors $Q = 4\pi/\lambda \sin(\theta/2)$ (with θ being the scattering angle) from 0.03 to 0.45 Å^{-1}: detector–sample distance 1.1, 5, and 20 m with collimation 8, 8, and 20.5 m, respectively. Samples were measured in quartz cells with 1 mm sample thickness at a temperature of 287 ± 0.5 K. The raw data were radially averaged, corrected for electronic background and empty cell scattering, and normalized to the scattering from water using standard ILL software. After these corrections, the data from the different experimental settings were merged without further changes and rebinned to a constant Q spacing of 0.0045 Å^{-1} for better lucidity. For interacting polydisperse droplets of number density n with uncorrelated size and position the normalized SANS intensity (scattering cross section per unit volume) $I(Q)$ (cm^{-1}) can be written as the product of the single droplet form factor $F(Q, R_w, d)$ and a structure factor $S(Q, \phi_{shs}, \epsilon, \tau)$:

$$I(Q) = n \cdot F(Q, R_w, d) \cdot S(Q, \phi_{shs}, \epsilon, \tau) + I_{inc}. \quad (1)$$

We used a form factor for a polydisperse core–shell spherical particle with R_w being the radius of the water core and d the thickness of the AOT shell (Chen 1986). The polydispersity in radii is expressed by a Schultz distribution (Kotlarchyk *et al* 1987). $S(Q, \phi_{shs}, \epsilon, \tau)$ denotes the structure factor for a hard-sphere fluid with a narrow attractive well (Baxter 1968, Menon *et al* 1991) and a hard-sphere volume fraction ϕ_{shs}. The perturbation parameter ϵ is defined as the ratio of the width of the attractive well to the total particle radius (hard-sphere radius plus attractive well). Here ϵ was held constant at 0.05 and only the stickiness parameter τ was varied by the fitting procedure. As we are mainly interested in the droplet form and size, results for the structure factor fit will not be discussed. Scattering curves were analysed using the NIST package for analysis of SANS and USANS (ultra-small-angle neutron scattering) data (Kline 2006). Scattering length densities of the different compounds were fixed to the theoretical values. The thickness of the AOT shell d was constrained to 9.1 ± 1 Å as determined by SANS at the oil–water interface (Nave *et al* 2000). The model curves are convoluted with the known instrumental resolution; this affects mainly the determination of the polydispersity (Grillo 2001). In accordance with the literature (Arleth and Pedersen 2001, Kotlarchyk *et al* 1982), fitted values for the polydispersity index of the radius lay between 15 and 24%.

[3] Deuterated AOT was purchased from Professor R Thomas, Oxford.

2.3. Neutron backscattering

The dynamic scattering function consists of coherent and incoherent contributions:

$$S(\mathbf{Q}, \omega) = S_{coh}(\mathbf{Q}, \omega) + S_{inc}(\mathbf{Q}, \omega), \quad (2)$$

where the coherent scattering function can be regarded as the inverse space–time Fourier transform of the density fluctuations and, similarly, the incoherent scattering function as the inverse space–time Fourier transform of the self-correlation function $G_s(\mathbf{r}, t)$. The incoherent scattering function can be written as

$$S_{inc}(\mathbf{Q}, \omega) = \frac{1}{2\pi} \int \exp\{i(\mathbf{Qr} - \omega t)\} G_s(\mathbf{r}, t)\, d\mathbf{r}\, dt. \quad (3)$$

Experimentally, the dynamic scattering function is probed (convoluted) with the experimental resolution function R of the spectrometer used:

$$S(\mathbf{Q}, \omega) = \int_{-\infty}^{\infty} S(\mathbf{Q}, \omega') R(\omega' - \omega)\, d\omega'. \quad (4)$$

The resolution is a peaked function of width $\Delta\omega$. $\Delta\omega$ determines how well the long-time limit of $G(\mathbf{r}, t)$ can be probed. This long-time limit is of special interest as it gives information about the type of motion. Thus one expects for a liquid no elastic scattering as $G_s(\mathbf{r}, t \to \infty) \to 0$, in contrast to a slow translational diffusion (e.g. at low temperature) or to spatially confined motions, for which one always expects elastic scattering. In order to decide whether there is a real elastic intensity, one needs a good instrumental resolution, as offered by neutron backscattering (BS) spectrometers. An overview of the dynamical processes in the sample as a function of temperature can be obtained by so-called elastic fixed-window scans in BS. These scans are carried out by keeping the initial and final wavevectors $k_i = k_f$ fixed and by counting neutrons as a function of the sample temperature, thus measuring the elastic intensity S^{el} as a function of temperature for $\omega = 0$.

As the energy width of the dynamic scattering function increases with increasing temperature, we expect the elastic intensity to decrease if the characteristic relaxation time becomes of the order of or shorter than the instrumental resolution.

Depending on the activation energy of the dynamic processes and/or the relaxation time distribution, the

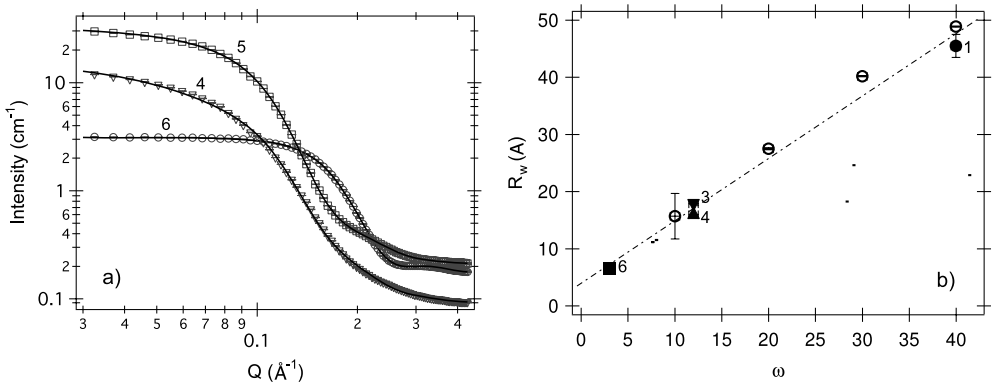

Figure 1. (a) Small-angle scattering profile of sample 6 (○), sample 5 (□) and sample 4 (▽) at $T = 287$ K; see table 1 for sample characteristics. Solid lines are fits to the form factor combined with structure factor model, as explained in section 2.2. (b) Water core radii R_w as a function of ω determined by small-angle scattering. Full symbols show results from SANS and hollow symbols are extracted from SAXS measurements. Numbers next to the symbols indicate the sample number as defined in table 1. The linear dependence of the radius on the molar ratio ω is shown by the dotted line.

observation is then a more or less sharp step of intensity in the temperature scan. In this work we report only on Q-integrated elastic intensities.

At high temperature the microemulsions are liquid, and the elastic incoherent scattering in the mentioned Q-range should go to zero if the energy resolution is good enough. However, for our microemulsions, which were 80 vol% deuterated, the coherent scattering is not negligible, and it will add to the elastic signal as well. One important contribution arises from the integrated coherent static structure factor.

We performed elastic fixed-window scans on the BS instruments IN16 and IN10. The good energy resolution of these spectrometers arises from Bragg angles of approximately 90°, used on both the Si(111) single-crystal monochromators and analysers ($\lambda = 6.271$ Å). With the given divergences and beam sizes this results in an energy resolution slightly better than $\sim$1 μeV FWHM (full width at half maximum). The corresponding time resolution can be estimated as $\tau \sim h/1\ \mu\text{eV} = 4$ ns or, if compared to a relaxation, as FWHM$/2/\omega \sim 1.3$ ns. For both instruments the accessible Q-range is given by the scattering angles covered by the analysers and the 22 (7) detectors of IN16 (IN10): $Q = 4\pi \sin(\Theta)/\lambda$ and extends from $Q \sim 0.2$ to 1.9 Å^{-1} at IN16 and from $Q \sim 0.4$ to 1.9 Å^{-1} at IN10.

Samples were measured in hollow aluminium cylinders with a 0.1 mm sample wall thickness sealed with indium. Samples were cooled from room temperature down below the freezing temperature of the oil and then heated again back to room temperature. Between 290 and 200 K (250 K for sample 1) cooling rates were 0.33 K min^{-1} and heating rates were 0.5 K min^{-1}. Raw data were treated using the *ILL* program *SQWel*, which corrects for scattering from the empty sample holder, self-shielding and normalizes the intensity to vanadium. Note that at low temperatures the samples are partially crystallized, and due to the resulting Bragg peaks we did not normalize to low-temperature intensity as is typically done for amorphous samples. Because calculated transmissions for all samples are of the order of 94%, no corrections for multiple scattering were applied.

3. Results and discussion

Before investigating the dynamical behaviour of the confined water it is crucial to determine the size of the confinement. Small-angle neutron scattering has been used to determine the droplet sizes of the microemulsions as a function of ω and ϕ. Whereas shell contrast microemulsions are normally better suited for structural investigations, due to their sharper contrast profile, we have prepared here full droplet and core contrast microemulsions because the very same samples were investigated in small-angle scattering and backscattering, which needs the high incoherent scattering cross section of the water protons. Different oils have been used to span a wide range of droplet sizes and also for changing the freezing point and the viscosity of the surrounding matrix. Whereas H_2O/AOT/toluene only forms a stable droplet microemulsion up to a molar ratio $\omega = 12$, and therefore restricts the droplet radius to about 20 Å, decane as oil allows for droplet radii up to 60 Å. On the other hand, decane crystallizes already around 240 K and thus the use of toluene or heptane, with freezing temperatures below 185 K, allowed us to expand the temperature range of the soft confinement to lower temperatures.

In figure 1(a) we show the SANS curves for samples 3, 4, and 6, for which the contrast is noted in table 1. The solid lines in figure 1 are fits to the form factor combined with the structure factor model as explained in section 2.2. The water core radii resulting from such fits are shown in figure 1(b) as a function of molar ratio ω, and are also tabulated in table 1. As expected from geometrical considerations (Kotlarchyk *et al* 1984), the radius depends approximately linearly on ω, as shown by the dotted line in figure 1(b). For a few cases, where we have no SANS measurements, we have relied on this linear interpolation. Additional results obtained by small-angle x-ray scattering (SAXS) on a H_2O/AOT/decane microemulsion with $\phi = 0.1$ are also included in the figure (Blochowicz *et al* 2007). These x-ray results confirm our SANS findings for the radius in a quantitative way. They show the possibility to use these ternary microemulsions for the investigation of

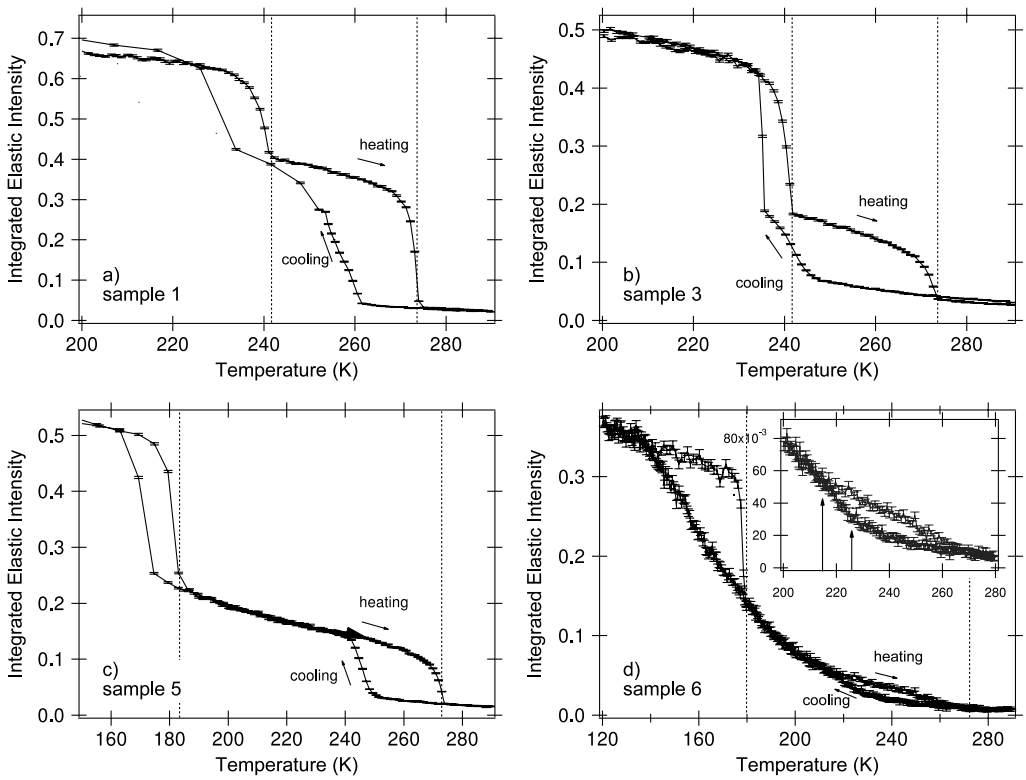

Figure 2. Elastic temperature scans of microemulsions with varying droplet sizes performed on IN16 (a)–(c) and IN10 (d). Dotted vertical lines show the freezing points of bulk water (273.2 K) and the oil ((a) and (b) deuterated decane, (c) deuterated heptane and (d) deuterated toluene). Droplet radii decrease from (a) 46 Å, (b) 18 Å, (c) 18 Å to (d) 7 Å.

Table 1. Summary of sample compositions and SANS and BS results: R_w denotes the radius of the water core, and ΔT is the difference between the observed freezing point of the confined water and bulk water. Values with * have not been measured with SANS, but the radii were deduced from linear interpolation.

Sample	Composition	SANS-contrast	ω	ϕ	R_w (Å)	ΔT (K)
1	H_2O/AOT/n-decane-d22	Full droplet	40	0.2	45.6 ± 0.5	15.5 ± 4.0
2	H_2O/dAOT/n-decane-d22	Water core	40	0.2	$^*45.6 \pm 1$	20.1 ± 4.9
3	H_2O/AOT/n-decane-d22	Full droplet	12	0.2	$^*17.9 \pm 1$	31.2 ± 4.0
4	H_2O/dAOT/n-decane-d22	Water core	12	0.2	17.9 ± 0.5	31.8 ± 4.4
5	H_2O/AOT/n-heptane-d16	Full droplet	12	0.2	16.0 ± 0.5	27.3 ± 3.7
6	H_2O/AOT/n-toluene-d8	Full droplet	3	0.2	6.62 ± 0.5	50.7 ± 3.5

water confinement, profiting from the fact that the size of the confinement can be continuously varied by changing the molar ratio ω of water to AOT. In figure 2, four out of the six elastic scans performed with similar contrast are shown. In addition, elastic scans for the pure n-decane-d22 and the AOT/n-decane-d22 system were carried out to better control the influence of the several constituents of this complex system. The temperature range that is displayed for the different samples was chosen in such a way that the freezing step of the oil is visible. The size of the microemulsion droplets decreases from (a) 46 Å, (b) 18 Å, (c) 18 Å to (d) 7 Å; see table 1 for a summary of the different microemulsion samples and their characteristics. For the elastic temperature scans shown, the intensity is summed over all 22 (7) detectors of IN16 (IN10) corresponding to the Q-range given above. Arrows indicate cooling and heating curves for the samples, and the dotted vertical lines indicate the freezing temperatures of bulk water and oil ((a) and (b): n-decane-d22, (c): n-heptane-d16, (d): toluene-d8), respectively. Below the freezing temperature of the oil the whole system can be considered as frozen, and with increasing temperature only vibrational motions lead to a slight decrease in intensity due to an average Debye–Waller factor. Following the scattering on the heating curve, a first steep drop in intensity occurs at the melting point of the bulk oil because the oil molecules move much more quickly than the time resolution of the instrument (note: coherent scattering, i.e. Bragg peaks and coherent short-range order scattering from the deuterated oil contribute in a few detectors as well). Upon further heating, a plateau region is observed, followed by a second steep drop at the melting temperature of bulk water (273.2 K), where all scatterers in the sample are too mobile for the energy resolution of the instrument. These two steps in the heating curves occur for all samples exactly at the temperatures where the bulk liquids (oil and water) do melt. It is noteworthy

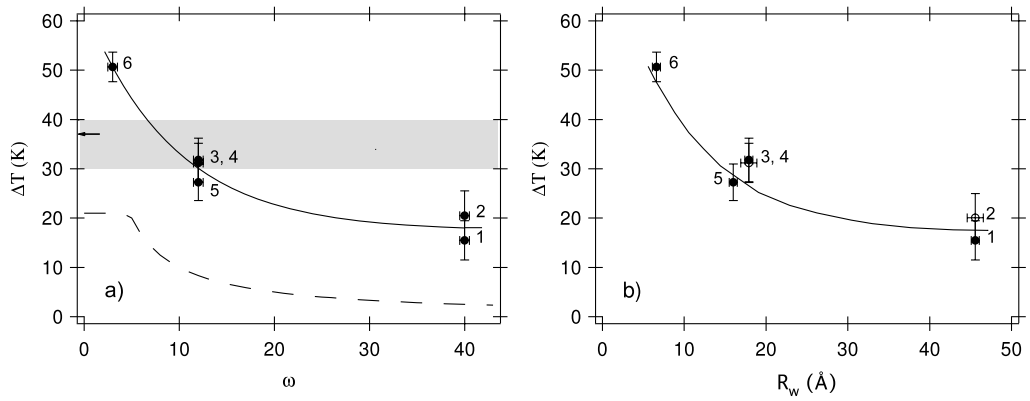

Figure 3. (a) The supercooling of the reverse micelle confined water as a function of ω; the solid line is a guide to the eyes. The dashed line indicates the possible supercooling caused by foreign dissolved particles. The grey rectangle shows the ω-independent range of supercooling of water as observed in a similar system (Nucci and Vanderkooi 2005); see text for further explanations. (b) The supercooling as a function of the radius; the full symbols show results from SANS measurements on the very same sample, and hollow circles are radii deduced from linear interpolation. Numbers next to the symbols indicate the sample number, as defined in table 1.

that upon heating there is no sign of crystallization of the water. This could be an indication for a gradual crystallization of the water upon cooling.

Focusing now on the elastic intensity upon cooling, one notices that the increase, corresponding to a freezing of water on the nanosecond timescale, is clearly shifted towards lower temperatures compared to the freezing point of bulk water. For sample 1, the biggest droplets investigated in this study, the elastic intensity increase caused by the freezing of water sets in at about 260 K. For the smaller droplet sizes investigated here, the freezing occurs at even lower temperatures and reaches for the smallest droplets (sample 6), with a radius of about 7 Å, a freezing temperature close to 220 K. Note that the homogeneous nucleation temperature of water lies at 236 K (Angell 1983); the corresponding amount of supercooling is shown by the arrow at the ΔT-axis in figure 3. For sample 6, with the smallest droplets, the elastic scan is not as unambiguous as the elastic scans of the samples with bigger droplets. Due to the relatively small amount of water, the step in intensity caused by the slowing down of the water molecules is, as expected, very small. Moreover, this scan has been performed on IN10, whose lower flux compared to IN16 complicates the interpretation of the scan due to the bigger errors. A clear change in slope of the integrated elastic intensity (indicated by the right arrow in the inset in figure 2(d)) led us to the conclusion that the water starts to freeze at this temperature.

It can furthermore be observed for all samples that freezing happens more gradually than melting, for which the elastic intensity drops more steeply. The amount of supercooling ΔT with respect to the bulk freezing temperature has been extracted in the following way. The beginning and end of the intensity step attributed to the water freezing were determined from the elastic scans (see arrows in figure 2(d)) and averaged. The width of the step is treated as the error of ΔT. The change in step height reflects the different relative amount of water but also the changing contrast with change in oil.

Figure 3(a) shows the amount of supercooling of the reverse micelle confined water as a function of molar ratio ω. The solid line is a guide to the eyes. It is clearly seen that the smaller the water to surfactant ratio ω the lower is the temperature at which we observe the freezing of water. As AOT is an anionic surfactant one also has to take into account the effect of the dissolved Na^+ ions. It is known that the freezing point of a salt solution is lower than the freezing point of the pure liquid. The cryoscopic constant of water is 1.86 K kg mol^{-1}. We estimate the upper limit for a shift of the freezing temperature caused by the AOT ions assuming that all AOT molecules are dissociated:

$$\Delta T_{\max} = \frac{1.86\ \text{K kg mol}^{-1}}{\omega \cdot m[\text{H}_2\text{O}]} \cdot 1000\ \text{g/kg} \qquad (5)$$

with $m[\text{H}_2\text{O}] = 18$ g mol^{-1} being the molar mass of water. For a saturated salt solution the maximal depression of the freezing point is 21 K. The resulting $\Delta T_{\max}$ as a function of ω is shown by the dashed line in figure 3. For all three sizes the water freezes at temperatures of more than 15 K below this. The salt concentration in the water cores can therefore not explain the large amount of supercooling of water that is observed.

The freezing behaviour of reverse micelle confined water has been investigated previously, and the results are contradictory. Mid-infrared spectroscopy was used to investigate the freezing behaviour of water in the droplets of a microemulsion consisting of water, AOT, and n-pentane with ω between 1 and 30 (Nucci and Vanderkooi 2005). Whereas they observe an ω-independent phase transition of the water occurring for all compositions in a interval between 335 and 245 K (indicated in figure 3(a)), there are also experimental results confirming our findings of a ω-dependent freezing point of water. Investigations using fluorescent probes were performed on water/AOT/n-heptane microemulsions with ω ranging from 5 to 20 (Munson *et al* 2004). This group found that the freezing point of water decreases with decreasing ω and is shifted from 263 K for $\omega = 20$ to 238 K for $\omega = 5$. In figure 3(b) the amount of supercooling is shown as a function

of water core radius. Stronger confinement leads to a bigger supercooling of the water. Comparison of sample 3, 4 and 5 with $\omega = 12$ shows that the viscosity of the surrounding oil matrix does not influence the freezing of water inside the droplets in a remarkable way. Freezing of the water in sample 3 and 4 (with n-decane-d22) and of the water in sample 5 (with n-heptane-d16) occurs within the error bars at the same temperature.

4. Conclusions

The freezing behaviour of reverse micelle water cores was investigated by means of elastic temperature scans on backscattering spectrometers. The radius of the water cores for $\omega = 40$, 12 and 3 has been determined by means of small-angle neutron scattering to be 46, 18 and 7 Å, respectively. It is found that the freezing point of reverse micelle confined water is depressed with comparison to bulk water. The observed supercooling cannot be explained by the dissociation of the anionic surfactant molecules. The amount of supercooling of the water increases with decreasing droplet size, confirming earlier results obtained by fluorescence probing (Munson *et al* 2004). This contradicts the finding of an ω-independent freezing point as reported by (Nucci and Vanderkooi 2005). Moreover, the influence of the viscosity of the surrounding oil was investigated by changing the oil from decane to heptane while keeping ω constant. It is found to be weak. It is shown that the ternary microemulsion consisting of water, AOT, and oil allows for the investigation of water in confinement over a wide range of temperatures down to where water exist in the supercooled state. The size of the confinement can be changed continuously by varying ω. These investigations on the nanosecond timescale lay the groundwork for ongoing dynamical investigations of confined water.

Acknowledgment

The Institute Laue Langevin is acknowledged for the beam time allocated.

References

Alba-Simionesco C, Coasne B, Dosseh G, Dudziak G, Gubbins K E, Radhakrishnan R and Sliwinska-Bartkowiak M 2006 *J. Phys.: Condens. Matter* **18** R15–68
Angell C A 1983 *Annu. Rev. Phys. Chem.* **34** 593–630
Arleth L and Pedersen J S 2001 *Phys. Rev.* E **63** 061406
Baxter R J 1968 *J. Chem. Phys.* **49** 2270–4
Blochowicz T, Gögelein C, Spehr T, Müller M and Stühn B 2007 *Phys. Rev.* E **76** 041505
Chen S H 1986 *Annu. Rev. Phys. Chem.* **37** 351–99
Christenson H K 2001 *J. Phys.: Condens. Matter* **13** R95–133
Grillo I 2001 *ILL Technical Report* p. ILL01GR08T
Kline S R 2006 *J. Appl. Crystallogr.* **39** 895–900
Kotlarchyk M, Chen S H and Huang J 1982 *J. Phys. Chem.* **86** 3273–6
Kotlarchyk M, Chen S H, Huang J and Kim M 1984 *Phys. Rev.* A **29** 2054–69
Kotlarchyk M, Stephens R and Huang J 1987 *J. Phys. Chem.* **92** 1533–8
Koza M, Frick B and Zorn R (ed) 2007 *3rd Int. Workshop on Dynamics in Confinement*; *Eur. Phys. J. Special Top.* **141**
Menon S V, Manohar C and Rao K S 1991 *J. Chem. Phys.* **95** 9186–90
Morineau D, Dosseh G, Alba-Simionesco C and Llewellyn P 1999 *Phil. Mag.* B **79** 1847–55
Munson C A, Baker G A, Baker S N and Bright F V 2004 *Langmuir* **20** 1551–7
Nave S, Eastoe J, Heenan R K, Steytler D and Grillo I 2000 *Langmuir* **16** 8741–8
Nucci N and Vanderkooi J 2005 *J. Phys. Chem.* B **109** 18301–9
Wang L, He F and Richert R 2004 *Phys. Rev. Lett.* **92** 095701